npg

p38MAPK inhibition: a new combined approach to reduce neuroblastoma resistance under etoposide treatment

B Marengo[1], CG De Ciucis[1], R Ricciarelli[1], AL Furfaro[1], R Colla[1], E Canepa[1], N Traverso[1], UM Marinari[1], MA Pronzato[1] and C Domenicotti*,[1]

Neuroblastoma (NB) is the second most common solid pediatric tumor and is characterized by clinical and biological heterogeneity, and stage-IV of the disease represents 50% of all cases. Considering the limited success of present chemotherapy treatment, it has become necessary to find new and effective therapies. In this context, our approach consists of identifying and targeting key molecular pathways associated with NB chemoresistance. This study has been carried out on three stage-IV NB cell lines with different status of MYCN amplification. Cells were exposed to a standard chemotherapy agent, namely etoposide, either alone or in combination with particular drugs, which target intracellular signaling pathways. Etoposide alone induced a concentration-dependent reduction of cell viability and, at very high doses, totally counteracted cell tumorigenicity and neurosphere formation. In addition, etoposide activated p38 mitogen-activated protein kinase (MAPK), AKT and c-Jun N-terminal kinase. Pre-treatment with SB203580, a p38MAPK inhibitor, dramatically sensibilized NB cells to etoposide, strongly reducing the dosage needed to inhibit tumorigenicity and neurosphere formation. Importantly, SB203580–etoposide cotreatment also reduced cell migration and invasion by affecting cyclooxygenase-2, intercellular adhesion molecule-1, C–X–C chemokine receptor-4 and matrix metalloprotease-9. Collectively, our results suggest that p38MAPK inhibition, in combination with standard chemotherapy, could represent an effective strategy to counteract NB resistance in stage-IV patients.
Cell Death and Disease (2013) **4**, e589; doi:10.1038/cddis.2013.118; published online 11 April 2013
Subject Category: Cancer

Neuroblastoma (NB) is the second most common pediatric solid malignant tumor and is characterized by biological and clinical heterogeneity.[1,2] While low-risk NB may spontaneously regress or differentiate into benign ganglioneuroblastoma, high-risk NB (stage-IV) results in metastatic dissemination[3] and only 20% of patients survive 5 years from diagnosis in spite of aggressive chemotherapy.[4]

Current therapeutic stratification of patients with NB is based on risk assessment according to combinations of age, tumor stage, MYCN status, DNA ploidy status and histopathology. This biological heterogeneity renders it necessary to identify additional markers for stratification and prognostication, as well as molecular pathways that can be targeted in combination with standard chemotherapy. However, the efficacy of the single-agent therapy is limited by mechanisms of resistance that hinder its clinical success. A factor that contributes to the malignancy of NB is the presence of a subpopulation of chemo- and radio-resistant stem cells in the tumor bulk.[5] These cancer stem-like cells (CSCs) contribute to both cancer progression and metastases. In NB, in fact,

neurospheres (NBSs), the CSCs of neuronal origin, have been found in primary tumor specimens, as well as in established cell lines.[6]

Moreover, it has been demonstrated that therapy-resistant aggressive NBs frequently overexpress and secrete high levels of growth factors and chemokines,[7] which are able to activate growth signaling pathways, thereby providing a suitable microenvironment for tumor development.[8,9]

In this study, we analyzed the main survival and death pathways triggered by etoposide, a commonly used chemotherapeutic compound, in two MYCN-amplified and one non-amplified cell lines. In particular, our study was strongly focused on HTLA-230, one of the MYCN-amplified NB cell lines, isolated from the bone-marrow aspirate of a patient with the stage-IV disease.[10] These cells are highly tumorigenic[11] and phenotypically similar to other metastatic bone marrow-isolated NB cells.[12]

Our results demonstrate that the etoposide resistance of NB cells is due to the presence of NBSs and suggest that SB203580, a specific p38 mitogen-activated protein kinase

(MAPK) inhibitor, in combination with etoposide, may be effective in preventing cell growth, invasion, migration, angiogenesis and NBS generation, which are all factors responsible for the relapse and progression of NB.

Results

Etoposide induces a dose-dependent reduction of cell viability and high doses totally counteract the tumorigenicity of NB cells and the formation of NBSs. NB cells were exposed for 24 h to increasing concentrations of etoposide (0.07–225 μM). As shown in Figure 1a, etoposide induced a dose-dependent reduction of cell viability, starting at a 10 μM concentration and reaching a 70% decrease at 225 μM. As shown in Figure 1b (left panel), untreated cells were able to form colonies (68 colonies of > 50 cells). Similarly, NB cells exposed for 24 h to 1.25 μM etoposide, a concentration that mimics *in vitro* the dose used in clinical therapy,[13] formed colonies (44 colonies of > 50 cells). On the contrary, higher doses of etoposide (from 10 to 225 μM) totally suppressed the clonogenicity of these cells.

Since the anchorage-independent growth is useful in detecting colonies, not appreciated by a clonogenic assay,[14] cells treated for 24 h with etoposide were grown in a semisolid agar. Similarly, as shown in Figure 1b (right panel), colonies were detected only in untreated samples (25 colonies of > 25 cells) and in 1.25 μM etoposide samples (16 colonies of > 25 cells).

When cells were plated above the clonal density (10 cells per μl) and grown under appropriate conditions, many NBSs were observed within 1 week in both untreated and 1.25 μM etoposide-treated cells (Figure 1c). Interestingly, the quantity of NBSs increased with the passage number (Figure 1c), but higher doses of etoposide (10–100 μM) prevented the formation of NBSs, already during the first week (Figure 1c).

As shown in Figure 1d, untreated and etoposide-treated monolayer cells expressed CD133 and Oct4, known stem cell markers.[15] Moreover, in NBSs, at the eighth passage, either originating from the control or from the treated cells, CD133 increased twofold, whereas Oct4 increased by 40 and 85% in untreated and treated NBSs, respectively (Figure 1d).

Since the effects on cell viability and clonogenicity, induced by 100 μM etoposide, were comparable to that induced by the higher doses, the subsequent analyses were performed until 100 μM.

At 24 h of treatment of cells with etoposide (10–100 μM) induced a dose-dependent increase of apoptotic cells and a necrotic effect was observed at 50 and 100 μM etoposide.

Etoposide produced a dose-dependent increase in dichlorofluorescein (DCF)-positive cells that became fivefold higher at 100 μM, and γ-H2AX, a marker of DNA double-strand breaks, was induced in etoposide-treated cells (data not shown).

Etoposide activates p38MAPK, AKT and JNK. As shown in Figure 2a, 24-h etoposide increased protein kinase C (PKC)δ and reduced PKCα levels. By analyzing the downstream molecular pathways of PKC, etoposide induced a dose-dependent activation of p38MAPK, already at 1.25 μM

(Figure 2b, left panel). In addition, c-Jun N-terminal kinase (JNK) was activated by 60 and 30%, at 1.25 and 10 μM, respectively, but no effect was observed at the other concentrations (Figure 2b, right panel). Moreover, etoposide increased the activity of Akt (phospho-Thr-Akt/Akt) by 70% in cells treated with the dose of 1.25 μM and by 50 and 35% (phospho-Ser-Akt/Akt), respectively, in cells exposed to 50 and 100 μM (Figure 2b, lower panel).

SB203580/etoposide cotreatment decreases cell viability, reduces the clonogenicity and inhibits the formation of NBSs. Since all signaling molecules analyzed were already activated at 1.25 μM etoposide, the effects of specific enzymatic inhibitors were investigated at this concentration of etoposide. As shown in Figure 3a (left panel), a reduction of cell viability was observed when etoposide-treated cells were pre-exposed to LY290042 (phosphatidylinositol 3-kinase (PI-3-kinase)/Akt inhibitor; 15% decrease), to SB203580 (p38MAPK inhibitor; 17% decrease) and to SP600125 (JNK inhibitor; 30% decrease). As shown in Figure 3a (right panel), while PD98059 (MEK inhibitor) pre-treatment increased the ability of NB cells to form colonies in the presence of etoposide, surprisingly, pre-treatment with SB203580 markedly reduced the tumorigenicity of etoposide-treated cells (60% decrease).

Treatment with the inhibitors that affected cell viability and tumorigenicity did not alter *per se* the number of NBSs (data not shown). As shown in Figure 3b, etoposide did not modify the number of NBSs, even in the presence of pre-treatment with LY290042 or SP600125 (first passage). However, when cells were pre-treated with SB203580 and then exposed to etoposide, the formation of NBSs was totally absent, even from the first passage (Figure 3b).

In addition, the progressive increase in NBSs observed in untreated, etoposide- and cotreated cells was dependent on passages and lasted for a period of 5 weeks (Figure 3b). After 6 weeks, the cotreatments did not change the number of NBSs (Figure 3b).

In the NBSs originating from untreated and etoposide-treated cells, p38MAPK was activated 18-fold compared with monolayer cells (Figure 3c, left panel), whereas the expression of MAPK phosphatase-1 (MKP-1), p38MAPK inhibitor, did not change (Figure 3c, right panel).

SB203580/etoposide or SP600125/etoposide cotreatments inhibit the formation of capillary-like structures. The ability of NB cells to form a network of tubes was not modified by etoposide or LY290042 after 24 h treatment (Figure 4a). Instead, SB203580 and SP600125 alone decreased the number of branches in the tube network by 55% with regard to untreated cells (Figure 4a, graph).

While the association of LY290042 with etoposide did not alter the formation of tubes, the cotreatment with SB203580 or SP600125 decreased the number of branches by 90% with regard to etoposide-treated cells (Figure 4a, graph). Moreover, tubes formed by untreated, etoposide- or LY290042-treated and cotreated cells persisted for up to 3 days. Similar results were observed in cells incubated in medium without basic fibroblast growth factor (bFGF) and vascular endothelial growth factor (VEGF) (data not shown).
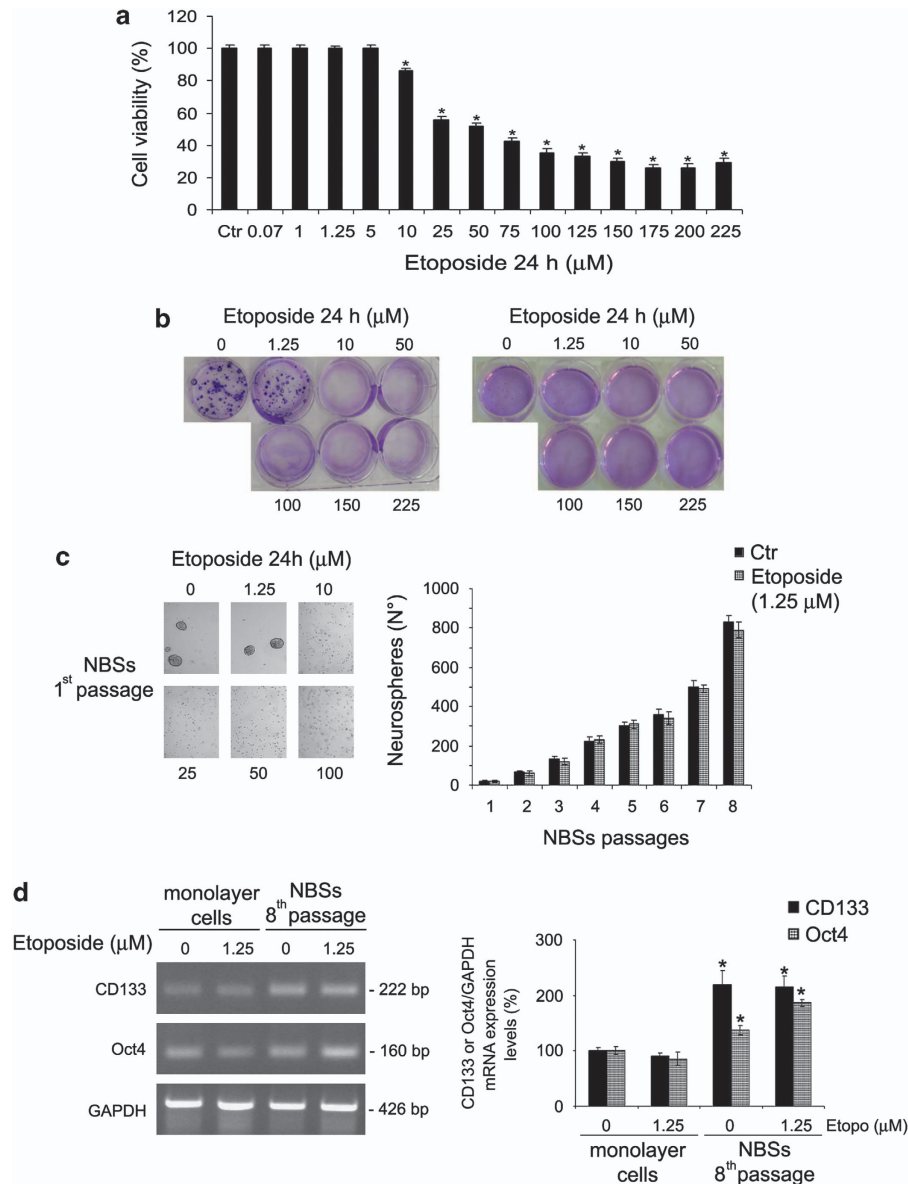
Figure 1 Etoposide decreases cell viability and, at high drug concentrations, inhibits the tumorigenic potential of HTLA-230 NB cells and prevents NBS formation. (**a**) Cell viability was determined by MTT assays in cells exposed to increasing concentrations of etoposide (0.07–225 μM) for 24 h. Histograms summarize quantitative data of means ± S.D. of five independent experiments. *$P < 0.01$ versus untreated cells (Ctr). (**b**) Left panel, clonogenic assay. HTLA-230 cells were seeded in six-well plates and then incubated with 1.25, 10, 50, 100, 150 and 225 μM etoposide, as indicated, for 24 h. Subsequently, cells were incubated in fresh medium without the drug for an additional 20 days before staining and counting the colonies. Right panel, soft-agar colony formation assay. HTLA-230 cells were treated with 1.25, 10, 50, 100, 150 and 225 μM etoposide, as indicated, for 24 h, washed and re-plated in agar-containing medium. After 25 days, colonies were stained and counted. (**c**) Left panel, NBS formation. After treatment with etoposide (1.25–100 μM), HTLA-230 cells were cultured in serum-free culture conditions containing bFGF and EGF for 1 week (first passage). Original magnification × 10. Right panel, graph. At every passage (one per week), the NBSs in untreated (Ctr) and in 1.25 μM etoposide-treated cells were counted by analysis under an inverted microscope. The histogram summarizes quantitative data of means ± S.D. of five independent experiments. (**d**) RT-PCR analyses of CD133 and Oct4 in untreated and etoposide-treated monolayer cells and in NBSs originating from by the same monolayer cells. The glyceraldehyde 3-phosphate dehydrogenase (GAPDH) signal is the internal loading control. Results are representative of three independent experiments with essentially similar results. Histogram, reported in the right panel, summarizes quantitative data of means, normalized to GAPDH expression ± S.D. of three independent experiments. *$P < 0.01$ versus monolayer cells

Furthermore, SB203580, alone or in combination with etoposide, reduced VEGF by 61 and 69%, respectively (Figure 4b). SP600125 alone was able to increase the VEGF amount twofold, but its combination with etoposide did not modify the VEGF expression (Figure 4b).

SB203580/etoposide cotreatment reduces cell migration and invasion by affecting COX-2, ICAM-1, CXCR4 expression and MMP-9 secretion. Cell migration was not altered by etoposide (Figure 4c) or by LY290042 or SB203580 or SP600125 administered alone (data not shown).
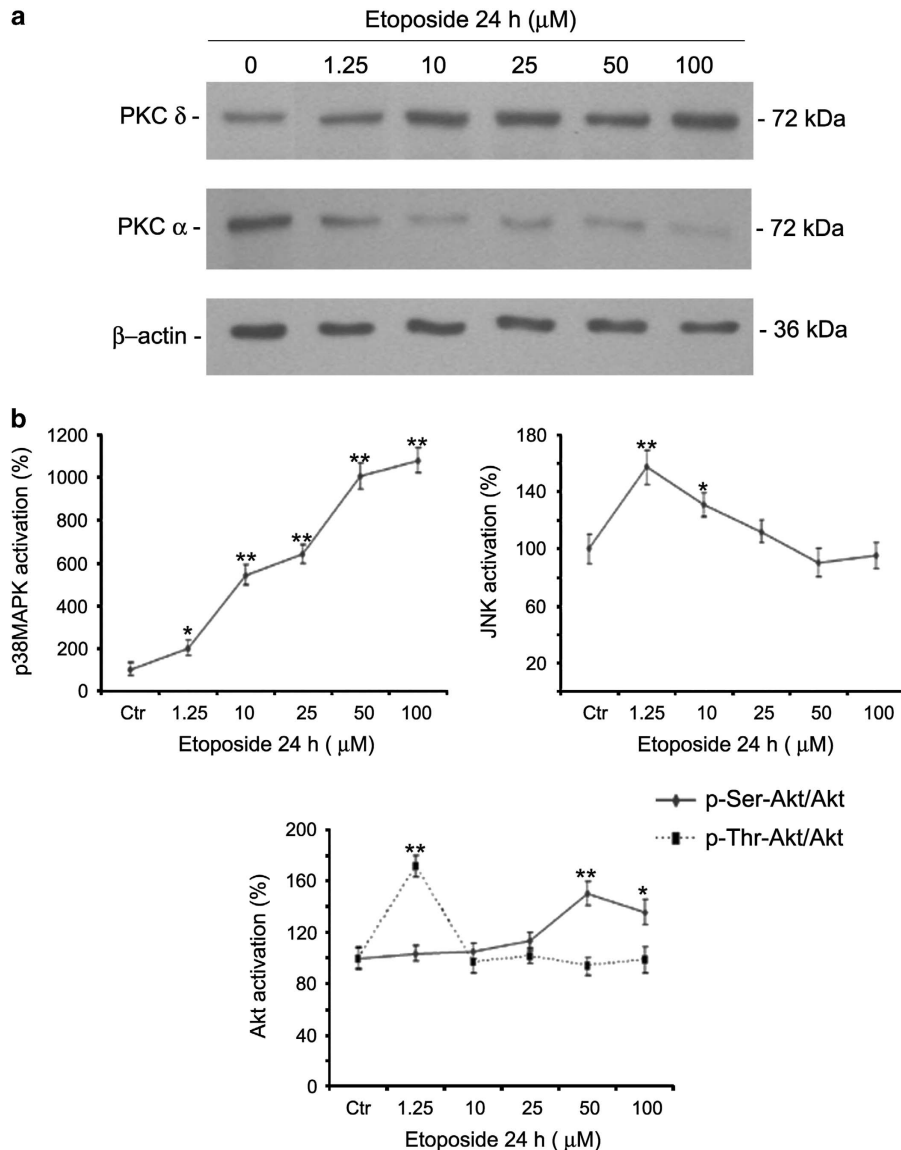
Figure 2 Etoposide activates p38MAPK, Akt and JNK. (**a**) Protein levels of PKC δ and α in cells treated with etoposide (1.25–100 μM). Immunoblots shown are representative of three independent experiments. β-Actin is the internal loading control. (**b**) p38MAPK, JNK and Akt activation. Histograms summarize quantitative data of means ± S.D. of three independent experiments. *$P < 0.05$ and **$P < 0.01$ versus untreated (Ctr) cells. Data are expressed as a ratio of the levels of phosphorylated proteins to the levels of unphosphorylated ones, whose values have been previously normalized against β-actin

Similarly, cotreatments of etoposide with LY290042 or SP600125 did not affect the cell migration (data not shown). It is worth noting that pre-treatment with SB203580 was able to reduce cell migration by 65% and 50%, evaluated by the scratch and Transwell assays, respectively (Figure 4c).

Cell invasion was reduced by 33% after etoposide treatment and was further inhibited by 51% and 80% after LY290042 and SB203580 cotreatments, respectively (Figure 4d). Moreover, SP600125 cotreatment did not change the number of membrane-invading cells (Figure 4d). LY290042 or SB203580 alone reduced the cell invasion by 34% and 60%, respectively, while SP600125 *per se* was uneffective (data not shown).

Considering the effects induced by SB203580 cotreatment on cell migration and invasion, some molecular markers, known to be related to the invasive phenotype, were investigated.

As shown in Figure 5a, etoposide induced a 60% increase in the cyclooxygenase (COX)-2 levels, an effect that was totally inhibited by the pre-treatment with SB203580. Moreover, treatment with SB203580 alone did not modify the COX-2 levels in untreated cells (Figure 5a).

Intercellular adhesion molecule-1 (ICAM-1) was reduced by 25% after etoposide and by 65% after SB203580 alone with regard to untreated cells (Figure 5b). Moreover, SB203580 cotreatment reduced the ICAM-1 levels found after etoposide by 40% (Figure 5b).
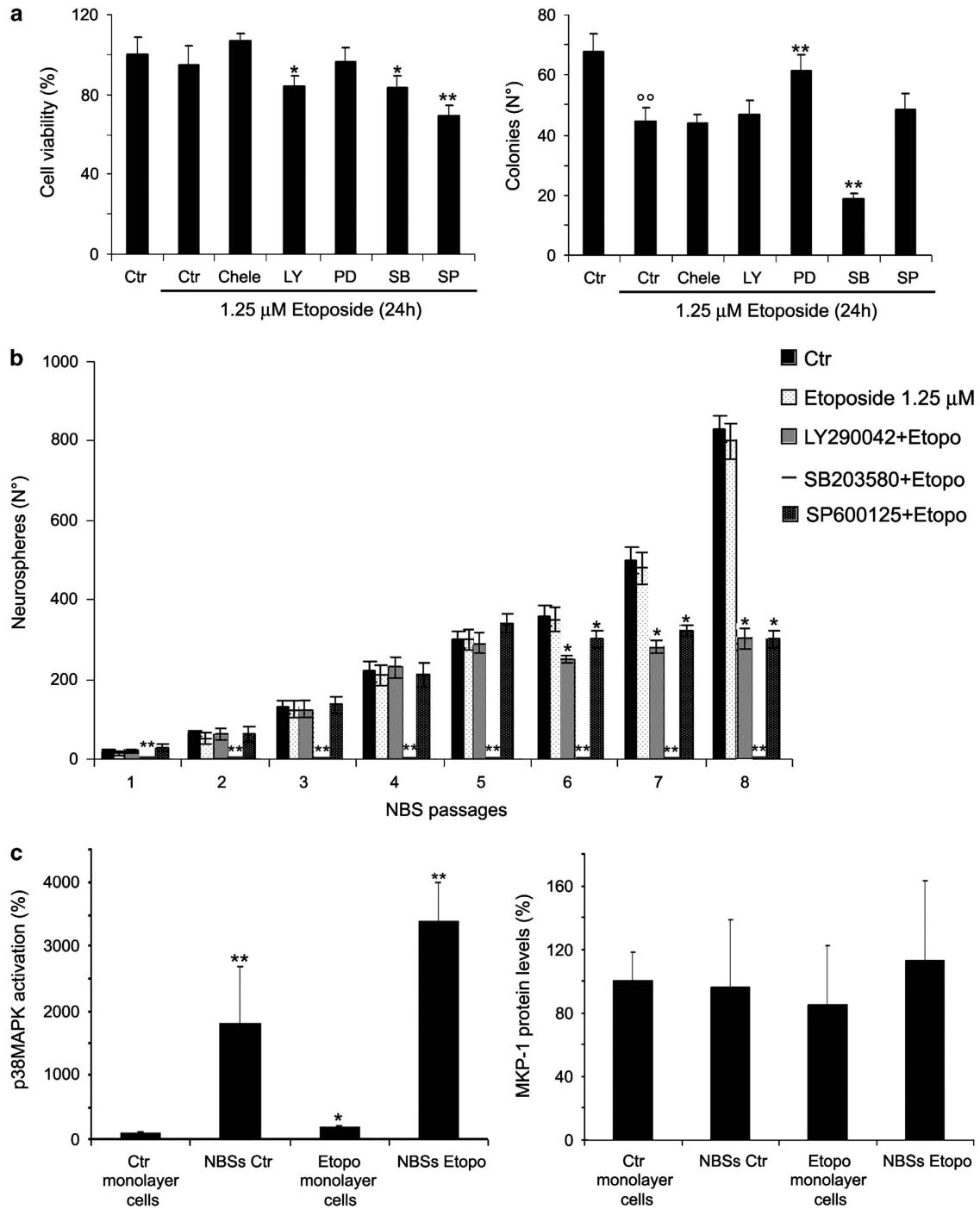
Figure 3 Effects of SB203580 (SB) cotreatment on cell viability, clonogenicity and formation of NBSs. (**a**) Left panel, cell viability. Cells were pre-treated for 1 h with the different inhibitors (0.1 μM chelerythrine chloride (Chele), 500 nM LY2940042 (LY), 50 μM PD98059 (PD), 10 μM SB203580 or 4 μM SP600125 (SP)) and then exposed to 1.25 μM etoposide for an additional 24 h. Histogram summarizes quantitative data of means $\pm$ S.D. of five independent experiments. *$P < 0.05$ *versus* etoposide-treated cells and **$P < 0.01$ *versus* etoposide-treated cells. Right panel, clonogenic assay. Histogram summarizes quantitative data of means $\pm$ S.D. of five independent experiments. $^{\circ\circ}P < 0.01$ *versus* untreated (Ctr) cells and **$P < 0.01$ *versus* etoposide-treated cells. (**b**) Growth curve of NBSs. At every passage (one per week), the NBSs originating from etoposide and inhibitor pre-treated cells were counted by analysis under an inverted microscope. Histogram summarizes quantitative data of means $\pm$ S.D. of three independent experiments. *$P < 0.05$ and **$P < 0.01$ *versus* etoposide-treated cells. (**c**) Left panel, p38MAPK activation in untreated monolayer cells and in NBSs. Histogram summarizes quantitative data of means $\pm$ S.D. of three independent experiments. *$P < 0.05$ *versus* untreated monolayer cells and **$P < 0.01$ *versus* monolayer cells. The data are expressed as a ratio of the levels of phosphorylated proteins to unphosphorylated proteins, whose values have been previously normalized with the relative glyceraldehyde 3-phosphate dehydrogenase (GAPDH) levels. Right panel, immunoblot analysis of MKP-1 in untreated monolayer cells and in NBSs. Histogram summarizes quantitative data of means $\pm$ S.D. of three independent experiments
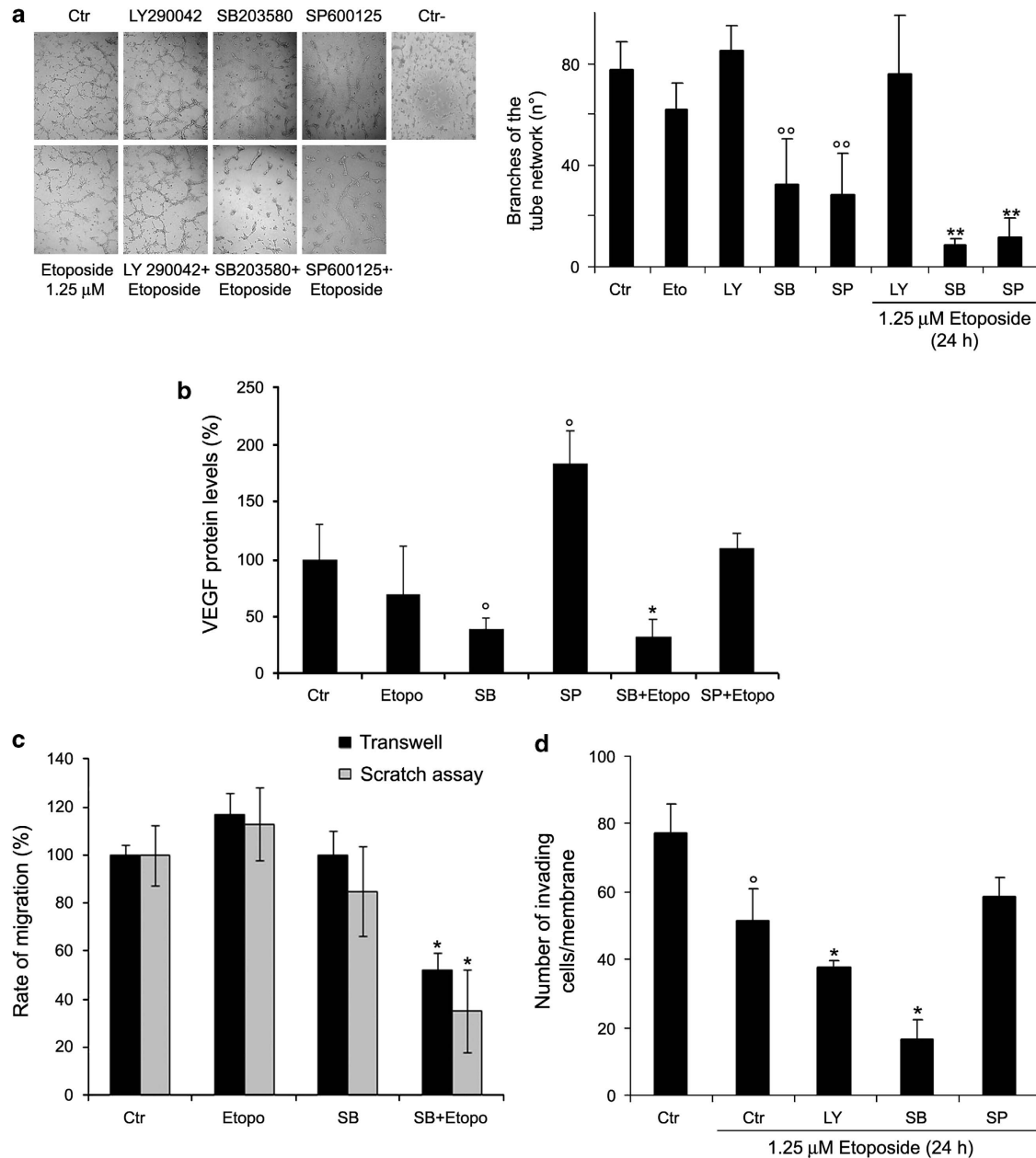
Figure 4 SB203580 (SB) or SP600125 (SP) inhibit the formation of capillary-like structures and SB203580 cotreatment reduces migration and invasion of etoposide-treated cells. (**a**) Formation of capillary-like structures. Representative micrographs of the complete network of tubes formed by untreated (Ctr), treated (with etoposide, LY2940042, SB203580 or SP600125 alone) and cotreated cells (etoposide plus inhibitors). The negative control is obtained by cell exposure to 10 μM sulforaphane. Original magnification $\times$ 10. The graph reports the number of branches of the tube network formed by cells under the treatment conditions as described above. Quantitative data are the means $\pm$ S.D. of three independent experiments. $^{\circ\circ}P < 0.01$ *versus* untreated (Ctr) cells and $^{**}P < 0.01$ *versus* etoposide-treated cells. (**b**) Immunoblot analysis of VEGF. The histogram summarizes quantitative data of means $\pm$ S.D. of three independent experiments $^{\circ}P < 0.05$ *versus* untreated (Ctr) cells and $^{*}P < 0.05$ *versus* etoposide-treated cells. The data are expressed as a ratio of VEGF to glyceraldehyde 3-phosphate dehydrogenase (GAPDH) amounts. (**c**) Migration assay. Cell migration was evaluated by the scratch and Transwell assays. In the scratch assay, the rate of migration was quantified by measuring the distance between the migrating cell boundaries. In the Transwell assay, migration was quantified by counting the number of cells, which moved to the underside of the membrane after 24 h of treatment. Histogram summarizes quantitative data of means $\pm$ S.D. of three independent experiments. $^{*}P < 0.01$ *versus* etoposide-treated cells. (**d**) Invasion assay. Cell invasion was quantified by counting the number of cells, which moved to the underside of the coated membrane after 24 h of treatment. Histogram summarizes quantitative data of means $\pm$ S.D. of six fields per membrane of three independent experiments. $^{\circ}P < 0.01$ *versus* untreated (Ctr) cells and $^{*}P < 0.01$ *versus* etoposide-treated cells

As shown in Figure 5c, etoposide or SB203580 alone did not alter the C–X–C chemokine receptor-4 (CXCR4) levels, while cotreatment was able to decrease the CXCR4 by 60%.

Analyses of matrix metalloprotease (MMP) activity demonstrated that MMP-9 was secreted by untreated cells (Figure 5d). In addition, etoposide or SB203580 alone did not influence the MMP-9 secretion (Figure 5d). However,
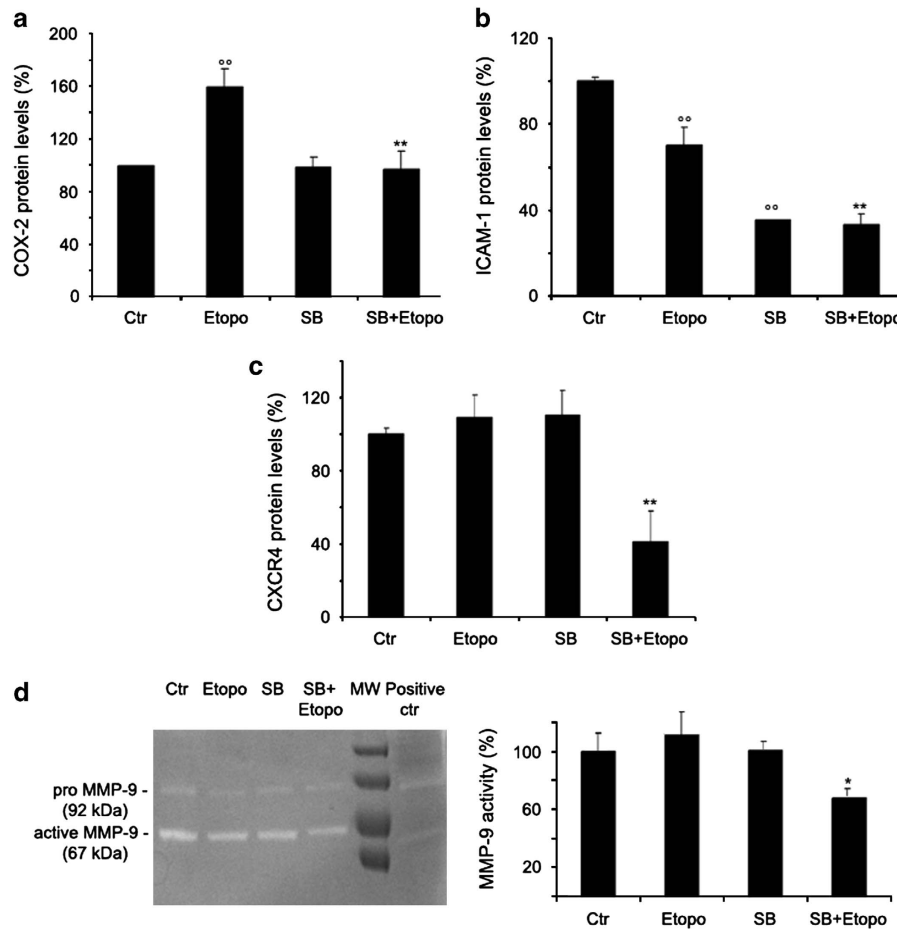
Figure 5 SB203580 (SB) reduces COX-2, ICAM-1, CXCR4 levels and MMP9 activity in etoposide-treated cells. Immunoblot analyses of COX-2 (**a**), ICAM-1 (**b**) and CXCR4 (**c**). The histograms summarize quantitative data of means ± S.D. of three independent experiments. $^{\circ\circ}P < 0.01$ versus untreated (Ctr) cells; $**P < 0.01$ versus etoposide-treated cells. The data are expressed as a ratio of COX-2 or ICAM-1 or CXCR4 to glyceraldehyde 3-phosphate dehydrogenase (GAPDH) amounts. MMP9 activity (**d**). Representative inverted black-and-white images of gelatin zymography are shown (left panel). The histogram (right panel) summarizes quantitative data of means ± S.D. of three independent experiments. The data are expressed as a ratio of pro-MMP9 to active MMP9. $*P < 0.05$ versus etoposide-treated cells

etoposide/SB203580 cotreatments reduced the release of MMP-9 by 33% (Figure 5d).

SB203580/etoposide decreases the viability of SK-N-SH and IMR-32 cells, reduces their tumorigenicity and inhibits the NBS formation only in IMR-32 cells. As shown in Figure 6a, etoposide induced a dose-dependent decrease in cell viability of SK-N-SH (without MYCN amplification) and of IMR-32 (with MYCN amplification). However, while the IMR-32 cell response to etoposide treatment was similar to that of HTLA-230 cells, SK-N-SH cells were more sensitive to the drug. In fact, 24-h etoposide, already at 1.25 μM, induced a reduction (of 30%) in cell viability of SK-N-SH (Figure 6a).

In addition, as shown in Figure 6b, the pretreatment of SK-N-SH with SB203580 caused a reduction of cell viability of 50% in regard to etoposide-treated cells, and sensitized IMR-32 cells, resistant to etoposide, by inducing a decrease of 48% in cell viability.

As shown in Figure 6c, etoposide alone decreased the number of colonies by 60% and 90% in SK-N-SH and IMR-32

cells, respectively. Moreover, in IMR-32 cells, SB203580 alone affected clonogenicity by reducing the clogenicity by 35% (Figure 6c). In both cell lines, the pre-treatment with SB203580 further reduced the tumorigenicity induced by etoposide (Figure 6c).

Untreated SK-N-SH and IMR-32 cells generated NBSs already within 1 week, and for each passage, the number of NBSs was equal to 30% of that originating from HTLA-230 (data not shown).

Etoposide or SB203580 alone totally inhibited the formation of NBSs in SK-N-SH but did not alter the number of NBSs in IMR-32 (data not shown). However, when IMR-32 cells were cotreated with SB203580 and etoposide, the formation of NBSs was totally prevented, even from the first passage (data not shown). As shown in Figure 6d, untreated and etoposide-treated monolayer SK-N-SH and IMR-32 cells expressed CD133 and Oct4 stem markers. Moreover, in NBSs, at the eighth passage, CD133 was markedly decreased (80–90%), whereas Oct4 did not change (Figure 6d).

In NBSs, originating from SK-N-SH and IMR-32 untreated cells, an activation of p38MAPK 7- and 11-fold, respectively,
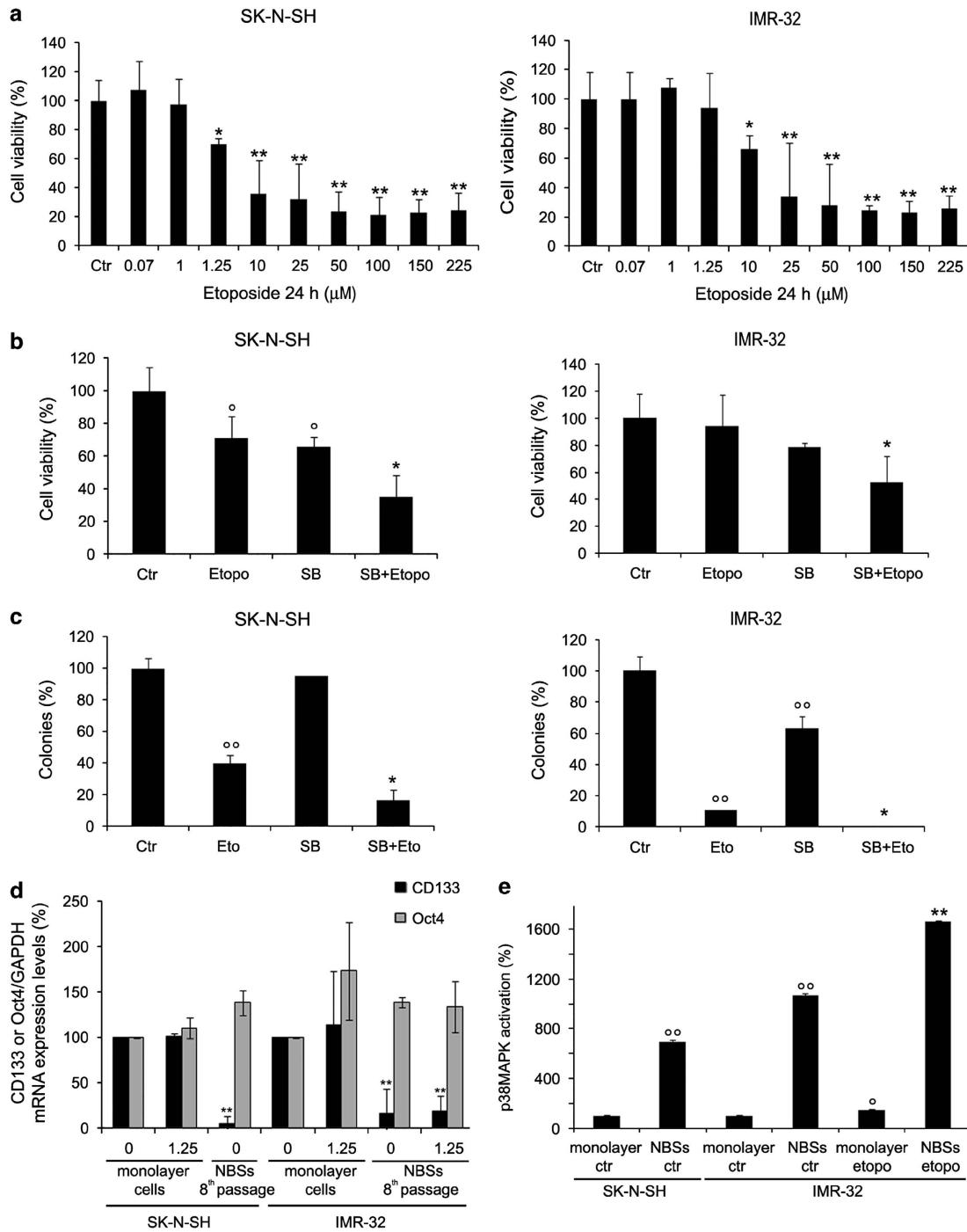
Figure 6 Effects of SB203580 (SB) cotreatment on viability, clonogenicity, CC133/Oct4 expression and p38MAPK activation in SK-N-SH and IMR-32 cells. (**a**) Cell viability. SK-N-SH (left panel) and IMR-32 (right panel) cells were exposed to increasing concentrations of etoposide (0.07–225 μM) for 24 h. Histograms summarize quantitative data of means ± S.D. of five independent experiments. *$P < 0.05$ and **$P < 0.01$ *versus* untreated cells (Ctr). (**b**) Cell viability. SK-N-SH (left panel) and IMR-32 (right panel) cells were treated with 1.25 μM etoposide/10 μM SB203580 alone or pre-treated for 1 h with 10 μM SB203580 and then exposed to 1.25 μM etoposide for an additional 24 h. Histogram summarizes quantitative data of means ± S.D. of five independent experiments. °$P < 0.05$ *versus* untreated cell (Ctr) and *$P < 0.05$ *versus* etoposide-treated cells. (**c**) Clonogenic assay. SK-N-SH (left panel) and IMR-32 (right panel) cells were seeded in six-well plates and then incubated with 1.25 μM etoposide/10 μM SB203580 alone or cotreated with SB203580 + etoposide for 24 h. Subsequently, cells were incubated in fresh medium without the drug for an additional 20 days before staining and counting the colonies. Histogram summarizes quantitative data of means ± S.D. of five independent experiments. °°$P < 0.01$ *versus* untreated cell (Ctr) and *$P < 0.05$ *versus* etoposide-treated cells. (**d**) RT-PCR analyses of CD133 and Oct4 in untreated and etoposide-treated monolayer cells and in NBSs originating from the same monolayer cells. The histogram summarizes quantitative data of means, normalized to glyceraldehyde 3-phosphate dehydrogenase (GAPDH) expression, ± S.D. of three independent experiments. **$P < 0.01$ *versus* monolayer cells. (**e**) p38MAPK activation in monolayer cells and in NBSs. Histogram summarizes quantitative data of means ± S.D. of three independent experiments. °$P < 0.05$ and °°$P < 0.01$ *versus* untreated monolayer cells and **$P < 0.01$ *versus* etoposide-treated monolayer cells. The data are expressed as a ratio of the levels of phosphorylated proteins to unphosphorylated proteins, whose values have been previously normalized with the relative GAPDH levels

was found in comparison to the monolayer cells (Figure 6e). Furthermore, in the NBSs from etoposide-treated IMR-32 cells, p38MAPK was activated eightfold compared with monolayer etoposide-treated ones (Figure 6e). No change in MKP-1 was observed (data not shown).

SB203580 plus etoposide decreases VEGF levels, markedly reduces cell migration/invasion and MMP-9 secretion. SK-N-SH and IMR-32 cells were unable to form capillary-like structures (Figure 7a). However, in these cell lines, etoposide alone reduced VEGF by 30% in SK-N-SH and by 15% in IMR-32 cells (Figure 7b). Similarly, SB203580 decreased VEGF by 38% in SK-N-SH and by 48% in IMR-32 cells (Figure 7b). In addition, SB203580, in combination with etoposide, further reduced VEGF by 20% and 50% in SK-N-SH and IMR-32 cells, respectively (Figure 7b).

As shown in Figure 7c, cotreatment of SB203580 with etoposide was able to reduce the cell migration of SK-N-SH by 77% and of IMR-32 cells by 40%, respectively (Figure 7c). In addition, etoposide and SB203580 alone were able to reduce cell migration of SK-N-SH by 45% and 40%, respectively (Figure 7c, left panel).

SB203580 alone or in combination with etoposide decreased by 80–83% the invasiveness of both cell lines (Figure 7d).

As shown in Figure 7e (left panel), etoposide or SB203580 alone reduced the secretion of MMP-9 from SK-N-SH cells by 30% and 75%, respectively. In IMR-32, etoposide did not influence the MMP-9 secretion (Figure 7e, right panel), while SB203580 alone reduced the MMP-9 release by 60% (Figure 7e, right panel). However, etoposide plus SB203580 reduced the release of MMP-9 by 22% in SK-N-SH and by 42% in IMR-32, with regard to cells treated with etoposide alone (Figure 7e).

Discussion

In this paper, we demonstrate that HTLA-230 and IMR-32, both MYCN-amplified cells, are highly etoposide-resistant, as only the doses ranging from 10 to 225 μM are able to reduce cell survival. In addition, HTLA-230 are more resistant than IMR-32 because 1.25 μM etoposide, a concentration that *in vitro* mimics the dose used in clinical therapy,[13] exerts a less marked antitumorigenic effect on HTLA-230, whereas the same dose of etoposide strongly decreases the clonogenicity of IMR-32 cells.

However, all NB cells analyzed are able to generate NBSs, but only in cells with MYCN-amplification, the treatment with etoposide does not interfere with NBS formation. These results are in agreement with a paper demonstrating that NBS-derived cells, originating from pediatric brain tumors, have an increased resistance to etoposide compared with monolayer-derived cells.[16] In addition, it has been demonstrated that only NB stage-IV-derived cells generate spheres, but that the MYCN expression status is not related to the sphere formation.[17]

In this paper, we demonstrate that in NBSs, originating from HTLA-230 cells, the levels of stemness markers (CD133 and Oct4) are enhanced, while in NBSs, originating from SK-N-SH and IMR-32 cells, the expression of CD133 is

reduced and Oct4 do not change. These results are in line with a report demonstrating that CD133 expression is increased in spheres but not in every analyzed sphere derived from NB samples and cell lines.[17,18] Probably, the overexpression of stemness markers contributes to rendering HTLA-230 more resistant to etoposide, and in this regard, it has been demonstrated that CD133 expression in NB cells is associated with resistance to doxorubicin, vincristine and cisplatin.[19]

In accordance with other studies,[20] we have recently reported that etoposide causes DNA damage and an overproduction of reactive oxygen species (ROS),[21] which have been demonstrated to mediate both cell damage and biological functions.[22] In this regard, herein we show that etoposide induces a dose-dependent increase in the levels of the proapoptotic PKCδ[23] and a parallel decrease of PKCα, the antiapoptotic isoform.[24]

However, given that PKCs are upstream molecules in the ROS signaling pathway leading to DNA damage and apoptosis,[21,25,26] it is important to identify the downstream mediators of the NB response to etoposide and we show that etoposide induces the activation of Akt and MAPKs (i.e. JNK, and p38). It is worth noting that the activation of MAPKs has been reported in over 50% of acute myelogenous and lymphocytic leukemia and that MAPKs are also stimulated in other tumors,[27,28] therefore implying that the inhibition of the MAPK pathways could represent an important strategy to counteract tumor growth. In this context, our results demonstrate that the viability of HTLA-230 exposed to 1.25 μM etoposide is reduced by the cotreatment with MAPKs and Akt inhibitors.

Moreover, cotreatment with etoposide and SB203580, a specific p38MAPK inhibitor, markedly reduces the tumorigenicity, while PD98059, an inhibitor of MEK, increases the ability to form colonies. These findings are in line with studies demonstrating, on the one hand, that p38MAPK activation plays a key role in tumorigenicity[29] and, on the other hand, that PD98059 fails to reduce the toxicity of etoposide.[30]

For the first time, we have demonstrated that SB203580, synergizing with etoposide, totally inhibits the formation of NBSs. This is probably related to the evidence that NBSs originating from MYCN-amplified cells have higher levels of p38MAPK activity in comparison to the same cells grown in monolayer and to NBSs originating from MYCN non-amplified cells. To confirm the fundamental role played by p38MAPK activation in CSC generation and propagation, the role of MKP-1, an endogenous inhibitor of MAPKs,[31] was investigated with the result that, in NBS cells, no changes were observed in MKP-1. Recently, it has also been demonstrated that p38MAPK activity enhances the expression of a specific subset of Oct4 target genes.[32] In this regard, SB203580 *plus* etoposide does not allow the formation of NBSs, probably due to its acting on CD133 and Oct4. Moreover, it has been found that CD133-positive cells maintain self-renewal and CSC-like properties by involving Oct4,[15] whose transcript is detected in many human carcinomas,[33] including NB.[11]

Noteworthy is that our data confirm previous evidence indicating that the p38 kinase is involved in the production of VEGF[34] and in VEGF-induced endothelial migration.[35] An additional mechanism of tumor angiogenesis is represented

by the vascular mimicry whereby cancer cells may acquire features that are typical of endothelial cells.[36] Recently, Pezzolo et al.[11] have suggested that targeting the ability of

HTLA-230 cells to transform into endothelial-like cells may counteract the contribution of NB-derived endothelial cells to tumor relapse and chemoresistance.[11] To our knowledge, our
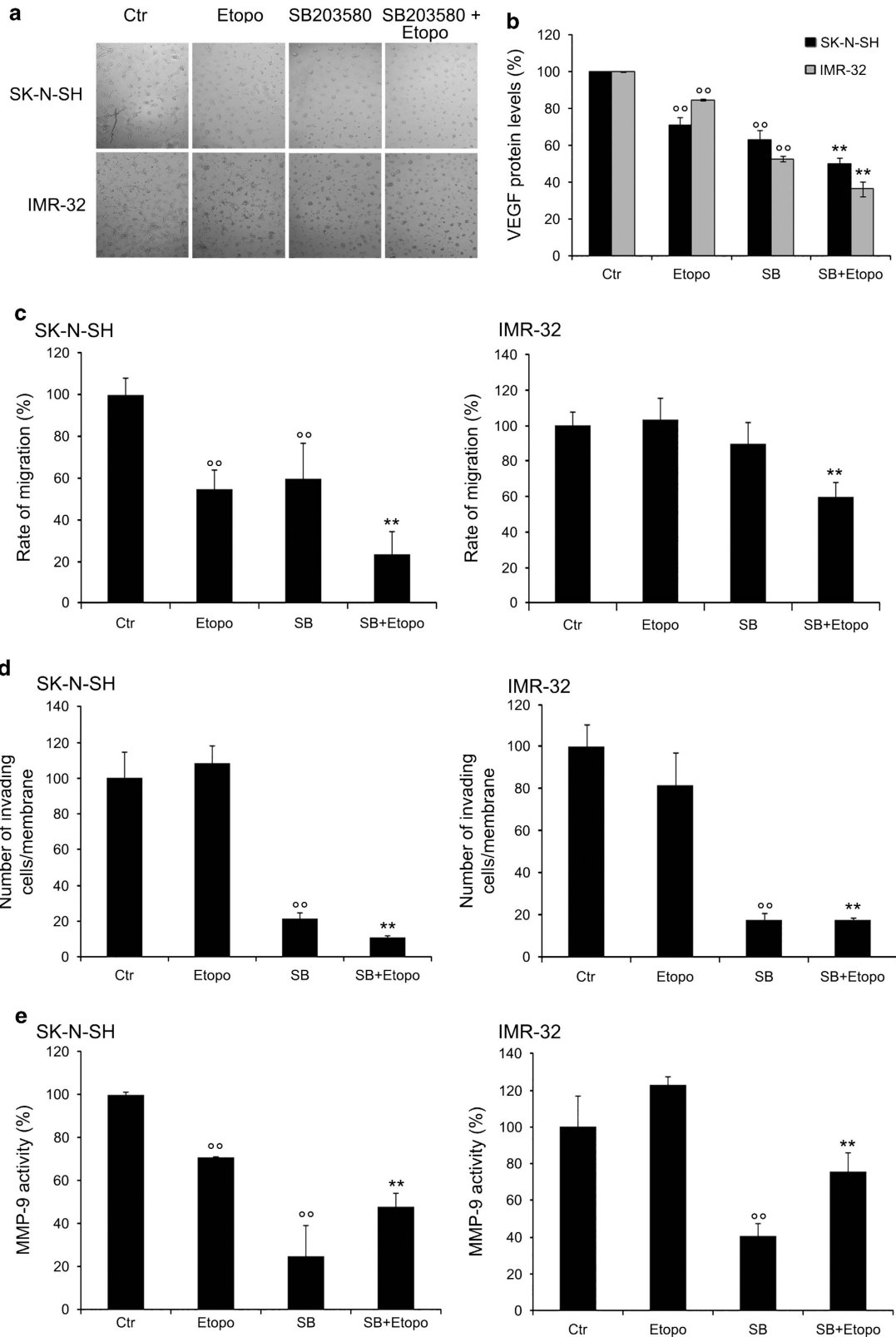
work is the first that demonstrates that the ability of untreated and treated HTLA-230 cells to acquire the typical features of endothelial cells is strongly reduced by p38MAPK and JNK inhibition. Moreover, our results demonstrate that p38MAPK inhibition decreases VEGF expression in all NB cells analyzed, suggesting that p38MAPK regulated VEGF via an MYCN-independent mechanism. However, considering that only SB203580 reduces VEGF in etoposide-treated cells, while both SB203580 and SP600125 inhibit vascular mimicry, it is possible that p38MAPK and JNK inhibitors may act by modulating other growth factors and matrix-related components.[37]

The p38MAPK pathway is known to regulate cancer development by modulating not only angiogenesis but also cell motility and invasion. In this context, our results demonstrate that migration and invasiveness of etoposide-treated NB cells is dependent on p38MAPK and also suggest that the inhibition of this pathway could be a new strategy in limiting the invasiveness of stage-IV NB. Accordingly, it has been demonstrated that SB203580 negatively affects, in vivo, breast cancer cell invasiveness,[38] whereas in vitro studies show that migration and invasion of bladder and hepatocarcinoma cells are linked to p38MAPK activity.[39,40]

Growing evidence also demonstrates that CXCR4, the chemokine stromal-derived factor 1 (SDF1/CXCL12) receptor, plays a key role in NB biology[41] and exerts a promigratory effect by activating p38MAPK.[42] Another modulator of the cancer invasiveness, whose expression is associated with the activation of MAPKs, is COX-2, (ref. 43–45) which increases migration and modulates the expression of the ICAM-1, an inducible surface glycoprotein that mediates adhesion-dependent cell-to-cell interactions.[46] In this regard, we have demonstrated that in HTLA-230 cells, etoposide markedly increases COX-2 expression according to the evidence that chemo/radiotherapies induce COX-2 in cancer.[47] On the other hand, etoposide reduces ICAM-1 and, although it does not affect cell survival, markedly reduces the cell invasiveness.

Probably, the effect of etoposide is the result of a balance between the increased expression of COX-2, linked to a major survival and migratory ability, and the reduced ICAM-1 expression, leading to a reduction of the metastatic potential of tumor cells. The cotreatment of etoposide with SB203580, by downregulating the expression of both proteins, on the one hand, determines a cytotoxic and antiangiogenetic effect and, on the other hand, reduces the invasive and metastatic properties. The demonstration that p38MAPK may regulate NB cell migration and invasiveness is confirmed by the inhibitory effect of SB203580 on the MMP-9 activity.

Therefore, these results strongly suggest that the combination of etoposide with SB203580 might be effective in blocking tumor growth and metastases.

Some preclinical studies have demonstrated that SB203580 is pharmacologically active in vivo in several animal models and is a potent inhibitor of cytokine production with only minor effects on the immune system.[48] Several p38 inhibitors tested for the treatment of inflammatory diseases have been well tolerated with minimal side effects.[49] Of particular note, there is increasing evidence that the different proinflammatory chemokines are implicated in the growth and invasivity of NB.[50]

In conclusion, we believe that, due to the dual activity on cancer cells and tumor microenvironment, standard chemotherapy combined with p38 inhibitors could represent a successful therapeutic strategy for the treatment of stage-IV NB.

Materials and Methods

Materials. Etoposide, chelerythrine chloride, LY2940042 and PD98059 were obtained from Calbiochem (Merck KGaA, Darmstadt, Germany). SB203580 and SP600125 were from Sigma Chemicals Co. (St. Louis, MO, USA). Matrigel (basement membrane matrix) was from Becton, Dickinson and Company (Franklin Lakes, NJ, USA).

Cell cultures and treatments. The MYCN-amplified human stage-IV NB cell lines, HTLA-230 and IMR-32, and the MYCN-non-amplified stage-IV SK-N-SH cells were obtained from Dr. V Pistoia (G Gaslini Institute, Genoa, Italy). The cell line was tested for mycoplasma contamination (Mycoplasma Reagent Set; Euroclone s.p.a, Pavia, Italy). Cell morphology and proliferation were analyzed after thawing and within eight passages in culture. Cells were cultured in RPMI1640 (Euroclone) supplemented with 10% fetal bovine serum (FBS; Euroclone), 2 mM glutamine (Euroclone), 1% penicillin/streptomycin (Euroclone), 1% sodium pyruvate (Sigma) and 1% of amino-acid solution (Sigma). Cells were treated for 24 h with etoposide doses ranging from 0.07 to 225 μM, and then, in a series of experiments, were pre-treated for 1 h with various enzymatic inhibitors of different signaling pathways: 0.1 μM chelerythrine chloride (PKC, pan inhibitor), 500 nM LY290042 (PI-3-kinase/Akt inhibitor), 50 μM PD98059 (MAP kinase kinase, MEK, inhibitor), 10 μM SB203580 (p38MAPK inhibitor) or 4 μM SP600125 (JNK inhibitor).

The stock solutions of etoposide and chemical inhibitors were prepared in DMSO and pilot experiments have demonstrated that the final DMSO concentrations did not change the cell responses analyzed.

MTT assay. Cell viability was determined using the dimethylthiazolyl-2-5-diphenyltetrazolium bromide (MTT; Sigma) staining. Briefly, cells were seeded into 96-well plates (Corning Incorporated, Corning, NY, USA) and then treated with etoposide and/or inhibitors for 24 h. Next, the cells were incubated with 0.5 mg/ml MTT for 3 h at 37 °C. After incubation, the supernatant was discarded, insoluble formazan precipitates were dissolved in HCl (0.1 N in isopropanol) and the absorbance at 570 nm was recorded using a microplate reader (EL-808; BioTek Instruments Inc., Winooski, VT, USA).

Figure 7 SB203580 cotreatment markedly reduces migration, invasion and MMP9 activity of etoposide-treated cells. (**a**) Formation of capillary-like structures. Representative micrographs of the complete network of tubes in untreated (Ctr) and treated cells. Original magnification × 10. (**b**) Immunoblot analysis of VEGF. The histogram summarizes quantitative data of means ± S.D. of three independent experiments °°$P < 0.01$ versus untreated (Ctr) cells and **$P < 0.01$ versus etoposide-treated cells. The data are expressed as a ratio of VEGF to glyceraldehyde 3-phosphate dehydrogenase (GAPDH) amounts. (**c**) Migration assay. Cell migration was evaluated in SK-N-SH (left panel) and IMR-32 (right panel) cells by the Transwell assay. Histogram summarizes quantitative data of means ± S.D. of three independent experiments. °°$P < 0.01$ versus untreated (Ctr) cells and **$P < 0.01$ versus etoposide-treated cells. (**d**) Invasion assay. Cell invasion was evaluated in SK-N-SH (left panel) and IMR-32 (right panel) cells and was quantified by counting the number of cells, which moved to the underside of the coated membrane after 24 h of treatment. Histogram summarizes quantitative data of means ± S.D. of six fields per membrane of three independent experiments. °°$P < 0.01$ versus untreated (Ctr) cells and **$P < 0.01$ versus etoposide-treated cells. (**e**) MMP9 activity. The histograms (SK-N-SH, left panel, and IMR-32, right panel) summarize quantitative data of means ± S.D. of three independent experiments. °°$P < 0.01$ versus untreated (Ctr) cells and **$P < 0.01$ versus etoposide-treated cells

Clonogenic assay. NB cells (150 per well) were seeded in six-well plates (Corning) and treated with etoposide and/or inhibitors for 24 h. Subsequently, the medium was changed and the cells were maintained in drug-free medium for 20 days. Cells were then fixed with methanol and stained with crystal violet (0.5% in water with 50% methanol). Colonies containing more than 50 cells were counted and the images were acquired with a Nikon Coolpix L22 camera (Nikon Corporation, Tokyo, Japan).

Soft-agar colony formation assay. NB cells were plated into six-well plates in the presence or absence of etoposide and/or inhibitors for 24 h. Anchorage-independent growth was carried out as follows: base agar (0.5% agar, RPMI1640 and 10% FBS) was added to each well and allowed to solidify, and then an equal volume of top agar (0.35% agar, RPMI1640 and 10% FBS), containing untreated or treated cells (10^3 cells per cm^2), was added to each well. Plates were incubated in a 5% CO_2 humidified incubator at 37 °C for 25 days. Colonies were stained with 0.005% crystal violet. Colonies containing more than 25 cells were counted by a Leica DMIRB microscope (Leica, Wetzlar, Germany) and the images were acquired with a Nikon Coolpix L22 camera (Nikon).

Sphere culture of NB cells. After treatment, NB cells were cultured in DMEM-F12 knockout medium (Invitrogen, Paisley, UK) containing 1% penicillin/streptomycin (Euroclone), 2% B27 supplement (Invitrogen), 40 ng/ml bFGF (R&D Systems Inc., Minneapolis, MN, USA) and 20 ng/ml epidermal growth factor (EGF; Invitrogen).[51] Half of the medium was then replaced with fresh culture medium every 7 days.

The self-renewal capacity of NBSs was determined by counting the spheres in the liquid culture. Growth curves were established by mechanically dissociating the passaged tumor spheres, plating 16×10^4 single cells in 25 cm^2 flasks and assessing the NBSs number at every passage.

RT-PCR analysis. Total RNA was extracted using TRIZOL reagent (Invitrogen) according to the manufacturer's instructions. Total RNA (1 μg) was reverse-transcribed into cDNA by random hexamer primer and SuperScript II Reverse Transcriptase (Invitrogen).

Amplification of cDNA by a polymerase chain reaction was performed using AmpliTaq Polymerase (Invitrogen) and specific primers for CD133, Oct4 and GAPDH. Primer sequences were: *CD133* Fw – 5′-ACATCTCAACATTAATGAGC-3′; CD133 Rv – 5′-TTTGCTTCTAGATCATATGC-3′(222 bp); Oct4 Fw – 5′-CAGT GCCCGAAACCCACAC-3′; Oct4 Rv – 5′-GGAGACCCAGCAGCCTCAAA-3′ (160 bp); GAPDH Fw–5′-AGCCACATCGCTCAGACACC-3′; and GAPDH Rv – 5′-TGAGGCTGTTGTCATACTTCTC-3′ (426 bp).

Fluorescence microscopy analysis of apoptotic and necrotic cells. For the assessment of apoptosis and necrosis, cells were analyzed as described previously.[25] Following treatment, cells were incubated with 0.5 μg/ml fluorescein isothiocyanate (FITC)-labeled recombinant Annexin-V and 0.5 μg/ml propidium iodide (PI; BioVision, Mountain View, CA, USA). Cells were then visualized and counted (four fields of 200–400 cells) by fluorescence microscopy using a Leica DMIRB microscope (Leica) with a dual filter set for FITC and rhodamine. Images were acquired with a Leica DCF320 camera. Cell death was evaluated as a percentage of Annexin-V (apoptotic) or PI-positive (necrotic) cells.

Detection of ROS production. Detection of ROS was performed as reported previously.[25] After treatment, cells were incubated with 20 μM 2′,7′-dichlorofluorescein-diacetate (DCFH-DA; Sigma) and the accumulation of DCF was analyzed at 530/485 nm. The cells were then observed and counted (four fields of 200–400 cells) by fluorescence microscopy using a Leica DMIRB microscope with a standard set of filters for fluorescein. The images were acquired with a Leica DCF320 camera.

DNA damage. Cells were seeded on chamber slides (Iwaky Seiyaku Co., Tokyo, Japan) treated with etoposide, fixed with paraformaldehyde (4% in PBS pH 7.5) and permeabilized with Triton 0.1%.

Nonspecific antibody binding was blocked by a 30 min incubation with 1% BSA and 1% gelatine. Cells were treated with anti-γ-H2AX antibody (1 : 500; Abcam, Cambridgeshire, UK) and then incubated with an FITC-conjugated anti-mouse antibody (Upstate, Lake Placid, NY, USA). Nuclei were identified by PI staining. Images were collected by fluorescence microscopy (Leica DMIRB microscope) with

a dual filter set for FITC and rhodamine. The images were acquired with a Leica DCF320 camera.

Immunoblot analysis. Immunoblots were carried out according to standard methods[25] using monoclonal mouse antibodies, anti-PKCα (Upstate, Lake Placid, NY, USA), anti-β-actin (Sigma), anti-γ-H2AX, anti-ICAM-1, anti-JNK (Abcam), anti-VEGF (Abnova, Taipei, Taiwan), and polyclonal rabbit antibodies, anti-human PKCδ, anti-Akt, anti-phospho-Akt (Thr308), anti-phospho-Akt (Ser473), anti-p38MAPK, anti-phospho-p38MAPK (Cell Signalling Technology Inc., Danvers, MA, USA), anti-phospho-JNK (Thr183) and anti-phospho-JNK (Tyr185), anti-CXCR4, anti-COX2 (Abcam), anti- MKP-1 and anti-GAPDH (Sigma).

Anti-mouse and anti-rabbit secondary antibodies were coupled with horseradish peroxidase (Amersham International, Buckinghamshire, UK). Proteins were visualized with an enzyme-linked chemiluminescence detection kit according to the manufacturer's (Amersham) instructions. Chemiluminescence was monitored by exposure to film and the signals were analyzed under non-saturating conditions with an image densitometer connected to Quantity One software (Bio-Rad Laboratories, Hercules, CA, USA).

Formation of capillary-like structures. *In vitro* formation of capillary-like structures was carried out on untreated and treated HTLA-230 cells (2×10^4 cells per well), seeded into a 96-Matrigel-coated well plate, adding endothelial basal medium in the presence or absence of VEGF (15 ng/ml) and bFGF (50 ng/ml).[11] In parallel, 10 μM sulforaphane was added as a control inhibitor of the capillary-like structure formation. Samples were analyzed over a 4–48 h period with a microscope (Leica DMIRB) using $\times$ 10 and $\times$ 20 lenses.

'Scratch' assay. HTLA-230 cells were plated into 24-well plates and cultured until confluent. A 200 μl pipette tip was used to 'scratch' the cell monolayers and then etoposide and/or inhibitors were added for 24 h. Photomicrographs were taken using an inverted microscope (Leica DMIRB) equipped with a $\times$ 10 lens. To evaluate the cell migration rate, images were recorded at time 0 and 24 h after the treatments. The distance between the two margins of the wound was analyzed by Adobe Photoshop 7.0.1.

Migration assay. Cell migration assay was carried out using the Transwell system (Corning) equipped with 8-μm pore size polycarbonate filters. Cells (5×10^4), suspended in serum-free medium, were plated into the upper chambers in the presence or absence of etoposide and/or inhibitors and allowed to migrate towards the lower chamber containing medium with 5% FBS, as a chemoattractant, for 24 h. Subsequently, the unmigrating cells in the upper compartment were removed using cotton swabs and the cells that had migrated to the lower surface of the filters were fixed with glutaraldehyde 2.5% (Sigma) and stained with Gill's hematoxylin no.1 solution (Sigma), following the manufacturer's instructions. The quantity of cells that had migrated through the filter was evaluated by microscopy analysis (Leica DMIRB microscope) using a $\times$ 10 lens.

Invasion assay. *In vitro* invasion assay was carried out in BD BioCoat Matrigel Invasion Chambers (BD) with 8 μm pores into 24-well plates, following the manufacturer's instructions. Cells (5×10^4), suspended in serum-free medium, were plated into the upper coated chambers in the presence or absence of etoposide and/or inhibitors and allowed to migrate towards the lower chamber containing medium with 5% FBS, as a chemoattractant, for 24 h. Subsequently, the unmigrated cells in the upper chamber were gently scraped off the filter. The quantity of cells that had migrated through the filter was evaluated by crystal violet staining and microscopy analysis (Leica DMIRB microscope) using a $\times$ 10 lens.

MMP activity. MMP activity in the conditioned media was determined by zymography, according to the methods described by Bernhard and Muschel.[52] Cells were cultured and treated in serum-free medium. Subsequently, the conditioned medium was harvested and centrifuged at 14 000 r.p.m. $\times$ 10 min at room temperature and the resulting supernatant was concentrated by using Amicon Ultra Centrifugal Filters (Millipore Ireland Ltd, Country Cork, UK). The total protein amount was determined by the BCA method (Pierce, Thermo Scientific, Rockford, IL, USA).

Substrate polyacrylamide gel electrophoresis was carried out by a modified protocol of Heussen and Dowdle,[53] using the gelatine Ready Gel Zymogram 10% (Bio-Rad Laboratories). Briefly, samples were mixed with Laemmli buffer (in a ratio of 3 : 1), warmed at 37 °C for 30 min and subjected to gel electrophoresis.

Subsequently, the gel was incubated for 48 h in developing buffer (50 mM Tris (pH 7.4), 0.2 M NaCl, 1% Triton X-100, 0.02 sodium azide and 5 mM $CaCl_2$).

After this step, the gel was stained for 1 h (0.2% Coomassie Blue, 30% ethanol and 10% acetic acid) and then de-stained in a solution containing 10% acetic acid. The gelatine digestion was analyzed with an image densitometer connected to Quantity One software (Bio-Rad Laboratories).

Data analysis. Results were expressed as mean ± S.D. from at least three independent experiments. The statistical significance of parametric differences among sets of experimental data was evaluated by one-way ANOVA and Dunnett's test for multiple comparisons.

Conflict of Interest

The authors declare no conflict of interest.

1. Brodeur GM. Neuroblastoma: biological insights into a clinical enigma. *Nat Rev Cancer* 2003; **3**: 203–216.
2. Maris JM, Hogarty MD, Bagatell R, Cohn SL. Neuroblastoma. *Lancet* 2007; **369**: 2106–2120.
3. Hansford LM, McKee AE, Zhang L, George RE, Gerstle JT, Thorner PS et al. Neuroblastoma cells isolated from bone marrow metastases contain a naturally enriched tumor-initiating cell. *Cancer Res* 2007; **67**: 11234–11243.
4. Tonini GP, Pistoia V. Molecularly guided therapy of neuroblastoma: a review of different approaches. *Curr Pharm Des* 2006; **12**: 2303–2317.
5. Jordan CT, Guzman ML, Noble M. Cancer stem cells. *N Engl J Med* 2006; **355**: 1253–1261.
6. Hirschmann-Jax C, Foster AE, Wulf GG, Nuchtern JG, Jax TW, Gobel U et al. A distinct 'side population' of cells with high drug efflux capacity in human tumor cells. *Proc Natl Acad Sci USA* 2004; **101**: 14228–14233.
7. Geminder H, Sagi-Assif O, Goldberg L, Meshel T, Rechavi G, Witz IP et al. A possible role for CXCR4 and its ligand, the CXC chemokine stromal cell-derived factor-1, in the development of bone marrow metastases in neuroblastoma. *J Immunol* 2001; **167**: 4747–4757.
8. Gerard C, Rollins BJ. Chemokines and disease. *Nat Immunol* 2001; **2**: 108–115.
9. Burger JA, Kipps TJ. CXCR4: a key receptor in the crosstalk between tumor cells and their microenvironment. *Blood* 2006; **107**: 1761–1767.
10. Matsushima H, Bogenmann E. Modulation of neuroblastoma cell differentiation by the extracellular matrix. *Int J Cancer* 1992; **51**: 727–732.
11. Pezzolo A, Parodi F, Marimpietri D, Raffaghello L, Cocco C, Pistorio A et al. Oct- 4 + / Tenascin C + neuroblastoma cells serve as progenitors of tumor-derived endothelial cells. *Cell Res* 2011; **21**: 1470–1486.
12. Castriconi R, Dondero A, Cilli M, Ognio E, Pezzolo A, De Giovanni B et al. Human NK cell infusions prolong survival of metastatic human neuroblastoma-bearing NOD/scid mice. *Cancer Immunol Immunother* 2007; **56**: 1733–1742.
13. Karlsson J, Ora I, Porn-Ares I, Pahlman S. Arsenic trioxide-induced death of neuroblastoma cells involves activation of Bax and does not require p53. *Clin Cancer Res* 2004; **10**: 3179–3188.
14. Franken NA, Rodermond HM, Stap J, Haveman J, van Bree C. Clonogenic assay of cells in vitro. *Nat Protoc* 2006; **1**: 2315–2319.
15. Chen YC, Hsu HS, Chen YW, Tsai TH, How CK, Wang CY et al. Oct-4 expression maintained cancer stem-like properties in lung cancer-derived CD133-positive cells. *PLoS One* 2008; **3**: e2637.
16. Hussein D, Punjaruk W, Storer LC, Shaw L, Othman R, Peet A et al. Pediatric brain tumor cancer stem cells: cell cycle dynamics, DNA repair, and etoposide extrusion. *Neuro Oncol* 2011; **13**: 70–83.
17. Khalil MA, Hrabeta J, Cipro S, Stiborova M, Vicha A, Eckschlager T. Neuroblastoma stem cells – mechanisms of chemoresistance and histone deacetylase inhibitors. *Neoplasma* 2012; **59**: 37–46.
18. Coulon A, Flahaut M, Muhlethaler-Mottet A, Meier R, Liberman J, Balmas-Bourloud K et al. Functional sphere profiling reveals the complexity of neuroblastoma tumor-initiating cell model. *Neoplasia* 2011; **13**: 991–1004.
19. Sartelet H, Imbriglio T, Nyalendo C, Haddad E, Annabi B, Duval M et al. CD133 expression is associated with poor outcome in neuroblastoma via chemoresistance mediated by the AKT pathway. *Histopathology* 2012; **60**: 1144–1155.
20. Oh SY, Sohn YW, Park JW, Park HJ, Jeon HM, Kim TK et al. Selective cell death of oncogenic Akt-transduced brain cancer cells by etoposide through reactive oxygen species mediated damage. *Mol Cancer Ther* 2007; **6**: 2178–2187.
21. Marengo B, De Ciucis C, Ricciarelli R, Passalacqua M, Nitti M, Zingg JM et al. PKCdelta sensitizes neuroblastoma cells to L-buthionine-sulfoximine and etoposide

22. inducing reactive oxygen species overproduction and DNA damage. *PLoS One* 2011; **6**: e14661.
22. Gopalakrishna R, Jaken S. Protein kinase C signaling and oxidative stress. *Free Radic Biol Med* 2000; **28**: 1349–1361.
23. Basu A, Woolard MD, Johnson CL. Involvement of protein kinase C-delta in DNA damage-induced apoptosis. *Cell Death Differ* 2001; **8**: 899–908.
24. Jiang XH, Tu SP, Cui JT, Lin MC, Xia HH, Wong WM et al. Antisense targeting protein kinase C alpha and beta1 inhibits gastric carcinogenesis. *Cancer Res* 2004; **64**: 5787–5794.
25. Domenicotti C, Marengo B, Verzola D, Garibotto G, Traverso N, Patriarca S et al. Role of PKC-delta activity in glutathione-depleted neuroblastoma cells. *Free Radic Biol Med* 2003; **35**: 504–516.
26. Marengo B, De Ciucis C, Verzola D, Pistoia V, Raffaghello L, Patriarca S et al. Mechanisms of BSO (L-buthionine-S,R-sulfoximine)-induced cytotoxic effects in neuroblastoma. *Free Radic Biol Med* 2008; **44**: 474–482.
27. Mebratu Y, Tesfaigzi Y. How ERK1/2 activation controls cell proliferation and cell death: Is subcellular localization the answer? *Cell Cycle* 2009; **8**: 1168–1175.
28. McCubrey JA, Steelman LS, Abrams SL, Bertrand FE, Ludwig DE, Basecke J et al. Targeting survival cascades induced by activation of Ras/Raf/MEK/ERK, PI3K/PTEN/Akt/mTOR and Jak/STAT pathways for effective leukemia therapy. *Leukemia* 2008; **22**: 708–722.
29. Sato T, Yamochi T, Yamochi T, Aytac U, Ohnuma K, McKee KS et al. CD26 regulates p38 mitogen-activated protein kinase-dependent phosphorylation of integrin beta1, adhesion to extracellular matrix, and tumorigenicity of T-anaplastic large cell lymphoma Karpas 299. *Cancer Res* 2005; **65**: 6950–6956.
30. Amran D, Sancho P, Fernandez C, Esteban D, Ramos AM, de Blas E et al. Pharmacological inhibitors of extracellular signal-regulated protein kinases attenuate the apoptotic action of cisplatin in human myeloid leukemia cells via glutathione-independent reduction in intracellular drug accumulation. *Biochim Biophys Acta* 2005; **1743**: 269–279.
31. Owens DM, Keyse SM. Differential regulation of MAP kinase signalling by dual-specificity protein phosphatases. *Oncogene* 2007; **26**: 3203–3213.
32. Saxe JP, Tomilin A, Scholer HR, Plath K, Huang J. Post-translational regulation of Oct4 transcriptional activity. *PLoS One* 2009; **4**: e4467.
33. Gidekel S, Pizov G, Bergman Y, Pikarsky E. Oct-3/4 is a dose-dependent oncogenic fate determinant. *Cancer Cell* 2003; **4**: 361–370.
34. Pages G, Berra E, Milanini J, Levy AP, Pouyssegur J. Stress-activated protein kinases (JNK and p38/HOG) are essential for vascular endothelial growth factor mRNA stability. *J Biol Chem* 2000; **275**: 26484–26491.
35. McMullen ME, Bryant PW, Glembotski CC, Vincent PA, Pumiglia KM. Activation of p38 has opposing effects on the proliferation and migration of endothelial cells. *J Biol Chem* 2005; **280**: 20995–21003.
36. Pezzolo A, Parodi F, Corrias MV, Cinti R, Gambini C, Pistoia V. Tumor origin of endothelial cells in human neuroblastoma. *J Clin Oncol* 2007; **25**: 376–383.
37. Paulis YW, Soetekouw PM, Verheul HM, Tjan-Heijnen VC, Griffioen AW. Signalling pathways in vasculogenic mimicry. *Biochim Biophys Acta* 2010; **1806**: 18–28.
38. Jang BC, Sanchez T, Schaefers HJ, Trifan OC, Liu CH, Creminon C et al. Serum withdrawal-induced post-transcriptional stabilization of cyclooxygenase-2 mRNA in MDA-MB-231 mammary carcinoma cells requires the activity of the p38 stress-activated protein kinase. *J Biol Chem* 2000; **275**: 39507–39515.
39. Kumar B, Koul S, Petersen J, Khandrika L, Hwa JS, Meacham RB et al. p38 mitogen-activated protein kinase-driven MAPKAPK2 regulates invasion of bladder cancer by modulation of MMP-2 and MMP-9 activity. *Cancer Res* 2010; **70**: 832–841.
40. Hsieh YH, Wu TT, Huang CY, Hsieh YS, Hwang JM, Liu JY. p38 mitogen-activated protein kinase pathway is involved in protein kinase Calpha-regulated invasion in human hepatocellular carcinoma cells. *Cancer Res* 2007; **67**: 4320–4327.
41. Raffaghello L, Cocco C, Corrias MV, Airoldi I, Pistoia V. Chemokines in neuroectodermal tumour progression and metastasis. *Semin Cancer Biol* 2009; **19**: 97–102.
42. Hiratsuka S, Duda DG, Huang Y, Goel S, Sugiyama T, Nagasawa T et al. C-X-C receptor type 4 promotes metastasis by activating p38 mitogen-activated protein kinase in myeloid differentiation antigen (Gr-1)-positive cells. *Proc Natl Acad Sci USA* 2011; **108**: 302–307.
43. Hwang D, Jang BC, Yu G, Boudreau M. Expression of mitogen-inducible cyclooxygenase induced by lipopolysaccharide: mediation through both mitogen-activated protein kinase and NF-kappaB signaling pathways in macrophages. *Biochem Pharmacol* 1997; **54**: 87–96.
44. Tsujii M, Kawano S, DuBois RN. Cyclooxygenase-2 expression in human colon cancer cells increases metastatic potential. *Proc Natl Acad Sci USA* 1997; **94**: 3336–3340.
45. Fulton AM, Ma X, Kundu N. Targeting prostaglandin E EP receptors to inhibit metastasis. *Cancer Res* 2006; **66**: 9794–9797.
46. Zimmerman T, Blanco FJ. Inhibitors targeting the LFA-1/ICAM-1 cell-adhesion interaction: design and mechanism of action. *Curr Pharm Des* 2008; **14**: 2128–2139.
47. Khan Z, Khan N, Tiwari RP, Sah NK, Prasad GB, Bisen PS. Biology of Cox-2: an application in cancer therapeutics. *Curr Drug Targets* 2011; **12**: 1082–1093.
48. Badger AM, Bradbeer JN, Votta B, Lee JC, Adams JL, Griswold DE. Pharmacological profile of SB 203580, a selective inhibitor of cytokine suppressive binding protein/p38

kinase, in animal models of arthritis, bone resorption, endotoxin shock and immune function. *J Pharmacol Exp Ther* 1996; **279**: 1453–1461.

49. Lee MR, Dominguez C. MAP kinase p38 inhibitors: clinical results and an intimate look at their interactions with p38alpha protein. *Curr Med Chem* 2005; **12**: 2979–2994.

50. Gross N, Meier R. Chemokines in neuroectodermal cancers: the crucial growth signal from the soil. *Semin Cancer Biol* 2009; **19**: 103–110.

51. Toma JG, McKenzie IA, Bagli D, Miller FD. Isolation and characterization of multipotent skin-derived precursors from human skin. *Stem Cells* 2005; **23**: 727–737.

52. Bernhard EJ, RJ Muschel. Ras metastasis, and matrix metalloproteinase 9. *Methods Enzymol* 2001; **333**: 96–104.

53. Heussen C, Dowdle EB. Electrophoretic analysis of plasminogen activators in polyacrylamide gels containing sodium dodecyl sulfate and copolymerized substrates. *Anal Biochem* 1980; **102**: 196–202.